

Anatomically Based Modeling

UCSC-CRL-97-10

Jane Wilhelms and Allen Van Gelder
University of California, Santa Cruz

April 15, 1997

Abstract

We describe an improved, anatomically based approach to modeling and animating animals. Underlying muscles, bones, and generalized tissue are modeled as triangle meshes or ellipsoids. Muscles are deformable discretized cylinders lying between fixed origins and insertions on specific bones. Default rest muscle shapes can be used, or the rest muscle shape can be designed by the user with a small set of parameters. Muscles automatically change shape as the joints move. Skin is generated by voxelizing the underlying components, filtering, and extracting a polygonal isosurface. Isosurface skin vertices are associated with underlying components and move with them during joint motion. Skin motion is consistent with an elastic membrane model. All components are parameterized and can be reused on similar bodies with non-uniformly scaled parts. This parameterization allows a non-uniformly sampled skin to be extracted, maintaining more details at the head and extremities.

Contents

1	Introduction	3
2	Background and Related Work	4
2.1	Modeling Deformable Materials in General	4
2.2	Modeling Soft Tissues on Articulated Bodies	5
2.3	Facial Modeling	5
2.4	Whole Body Modeling	6
3	The Basic Model	6
3.1	Skeleton and Generalized Tissue	7
4	Muscles	7
4.1	Deformed Cylinder Model for Muscles	7
4.2	Setting the Default Muscle Shape	9
4.3	Non-Default Muscle Shapes	10
4.4	Muscle Animation	11
5	Skin	11
5.1	Anchoring Skin	12
5.2	The Elastic Model	13
5.3	Non-Uniform Scaling and Re-usability	15
6	Results and Discussion	15
7	Future Work	16
8	Conclusions	17

1 Introduction

Humans, and other animals, are among the most important and interesting objects simulated using computer graphics, but they are also the most difficult to realistically model and animate. They are important because computer simulations of them provide insights into medical, biomechanical, sports, and ergonomic problems, make virtual reality applications more realistic, provide a means to safely include humans and animals (real, imaginary, and extinct) in motion pictures and advertising, and indicate useful control strategies for robotics. They are interesting because they are beautiful, varied, and capable of more engaging behavior than plants and machines. They are very difficult to model because they are complex, having many moving joints and billions of soft cells. They are even harder to animate because their motion is finely controlled and coordinated, and their control methodology is even now not well understood.

In general, computer graphics has achieved greater realism by developing methods that *simulate* the real world, rather than using ad hoc methods. As a step in this direction, we present a modeling and animation approach that is more closely based on anatomical principles than previously described methods. This model consists of individual muscles, bones, and generalized tissues covered by an elastic skin. The components mimic actual components of the animal body.

In real animals, muscles stretch across joints to cause motion, and skin movements caused by underlying muscles can occur across a wide area. In those with well-developed muscles, it is possible to actually identify individual muscles in motion. For simulated animals (and humans) to appear realistic, these widespread skin effects must be seen, and what better way to simulate these effects than to actually model individual muscles?

Our modeling approach involves the following steps:

1. A body hierarchy of segments and joints is specified and a rest position given for the joints;
2. Individual muscles, bones, and generalized tissues (the underlying components) are designed to give the body shape;
3. The underlying components are voxelized into a 3D grid, the grid is filtered to smooth irregularities, and a skin is extracted using isosurface techniques;
4. Skin vertices are mapped parametrically from world space into the coordinate system of the underlying component to which they are closest. Skin is modeled as an elastic material which in turn is approximated as a spring mesh. Rest lengths and spring constants are stored for each edge.

Animation involves repetition of the following steps:

1. Motion at joints is specified;
2. New positions of bones, generalized tissue, and muscles are calculated. Muscle lengths may change due to change in the distances between their origins and insertion points (see Section 4 for terminology). Muscle shapes are deformed appropriately to preserve volume.
3. Skin vertices are mapped from local component space to world space, taking into account joint motion and muscle deformation.
4. An iterative relaxation algorithm adjusts position skin vertices to achieve equilibrium of the elastic membrane forces.

The remainder of the paper is organized as follows: Background and related work are discussed in Section 2. The basic anatomically based model is described in Section 3. Technical details of muscles

and skin are discussed in Section 4 and Section 5. Results are evaluated in Section 6, and future work is discussed in Section 7. Conclusions are drawn in Section 8. A shortened version of this paper has been published [WVG97]. Examples from our work on anatomically based modeling can be found on our web site www.cse.ucsc.edu/~wilhelms/fauna.

2 Background and Related Work

Human and animal models of considerable complexity are being produced, but rarely would one confuse them with the real thing. In most cases, including the memorable dinosaurs and bears seen in commercial animations [Car94, SD93], initial material models were digitized and animated laboriously by trained people. Creating realistic models and animations involves enormous expense in time and compute power, as well as artistic and technical training. In most cases, the chief aim is verisimilitude, so the underlying model and animation do not represent actual body constituents.

Articulated bodies such as humans, other animals, and robots are almost universally modeled using a tree-structured hierarchy of rigid segments (sometimes called links) connected by joints that bear a more or less close relationship to the skeleton in animals [BZ91, BPW93, MTT93]. The hierarchy itself only provides for motion at joints, but such a model would appear at best like a jointed plastic doll – fairly realistic for a single position but obviously not correct when seen moving. For certain applications, such as ergonomics (where issues such as reachability and comfort are central), a high level of realism isn’t necessary, but in general it is desirable.

2.1 Modeling Deformable Materials in General

Modeling soft body tissues such as muscles, viscera, and fat is a special case of the larger problem of modeling deformable materials in general. Deformable materials may be represented as three-dimensional solids, or just a two-dimensional surrounding surface. Because these materials deform, their animation is deeply integrated with their modeling. *Kinematic* methods only consider positions taken; *dynamic* methods (also called *physical simulation*) consider the underlying physics. Kinematic methods include specifying key positions and interpolating [KCP92]; applying deformation transformations to analytical models [Bar84]; deforming a discretized model of space around the object parameterized within it (*free-form deformations*) [SP86]; and *implicit surfaces* (*isosurfaces*) [Bli82, WMW86, LC87, Blo88, DG95]. *Implicit* or *iso-surfaces* are basically equivalent, each being a two-dimensional surface of constant value within a three-dimensional scalar field. Implicit fields can be used to extract an outer surface around an object or to animate deformable materials (by moving the generative particles that define the field relative to each other, causing the field function to change).

The isosurface for a given threshold value in the field can be extracted by a wide variety of approaches. Blinn extracted it during rendering [Bli82]. Many methods assume or create a voxel space (*voxelization*) [WMW86, LC87, Blo88]. In voxelization, a three-dimensional grid of sample data values is created over the underlying field [WK94]. Voxelized representations suffer from the usual discretization problems, which can to some extent be dealt with by filtering [MN88]. The “marching-cubes” extraction approach is simple and fast [WMW86, LC87]. Physically based approaches have been used [dFdMGTV92, WH94]. The field may be sampled with particles [WH94, HDD⁺93, ST92, Tur92], or a closed geometric model may be adjusted to match the desired iso-curve or surface [KWT88, TPBF87, MBL⁺91]. If the number of points defining the surface is prohibitively large, it can be reduced using hierarchical methods [SBD86, Tur92] or mesh decimation [SZL92, HDD⁺93].

Physical simulation of deformable material involves creating a discretized version of the continuous

material as a mesh of connected point masses (*finite element meshes*) [TPBF87, PB88, TF88, MTT91, CZ92, TT94]. In the simplest case, connections are springs and dampers [Mil88]. In more sophisticated approaches, more expensive methods using elasticity theory are used [TPBF87, TW88].

2.2 Modeling Soft Tissues on Articulated Bodies

Relatively simple approaches have been used for modeling soft deformable tissue on an articulated body because of the complexity of the models involved. Muscles, skin, or other soft tissues are generally attached only to the nearest body segment. This can cause joints to appear unnatural [Cat72, FB88]. Badler *et al.* mimicked deformable material in early work by covering the body with many spheres [BOT79], while Herbison-Evans used ellipsoids to represent each segment [HE78]. Blinn’s seminal work on implicit surface modeling included a “blobby man” made by extracting a surface from around an articulated skeleton [Bli82]. Gascuel extracted a spline surface around a skeleton [Gas89]. Sometimes the surface is geometrically adjusted during motion to mimic deformation [HHS87]. Magnenat-Thalmann and Thalmann extended this idea in their joint-local deformations (JDL’s) where procedures are associated with each joint to simulate natural changes [MTT91]. Singh *et al.* presented an approach using implicit surfaces [SOP95].

Chadwick, Haumann, and Parent presented a method for layered construction of flexible animated characters [CHP89] using *free-form deformations* [SP86]. The free-form deformation approach was also used by Komatsu [Kom88] for skin. Mark Henne used a layered approach [Hen90], in which *implicit fields* simulated body tissue. Turner *et al.* use an elastic skin model for character animation [TT93]. Skin wrinkling has been explored by Wu *et al.* [WKT96]. Gourret *et al.* [GMMT89] used a finite element method to model the hand during grasping. None of these methods attempted to model individual three-dimensional muscles.

Chen and Zeltzer presented a biomechanically based muscle model using a finite element method to realistically simulate a few individual muscles without an overlying skin [CZ92]. The muscles were modeled using polyhedral meshes and a biomechanical contraction model used to calculate non-linear forces at mesh points. The cost would be prohibitive for the whole body at present. At some point, hopefully, computational resources will make it possible for animation and biomechanical simulation to converge further.

Another example from biomechanics is the work of Delp and Loan [DL95]. Bone surfaces, joint kinematics, lines of action, and forces caused by muscles can be specified. The function of muscles is analyzed by computing such parameters as length, moment, forces and torques. Using computer graphics, the user can view the model in three-dimensions and manipulate kinematics and geometry.

Recent work by Scheepers *et al.* is most closely related to ours [SPCM97]. Their emphasis is on modeling musculature, using a variety of geometric primitives.

2.3 Facial Modeling

The most anatomically detailed simulations have been done for the human face. Facial expressions are so complex and meaningful that doll-like rigidity is not acceptable [PB81, Par82, Wat87, TW90, TW93, LTW95]. Skin is generally modeled as a surface mesh whose points must move as expression changes. Early geometric models soon became parameterized [Par82] to allow higher level control over the number of skin vertices. Facial skin vertices were geometrically adjusted to mimic the actions of facial muscles [PB81, Wat87]. Physical simulation was integrated into facial modeling by Terzopoulos and Waters [TW90, TW93]. Lee *et al.* [LTW95] used a highly automated physics-based approach where a triangulated facial mesh from scanned data was combined with a fatty-tissue/muscle layer and a bone layer, which were connected by springs. Koch *et al.* also describes a system for simulating facial surgery using finite element models [KGC⁺96]. None of these models used individual muscles with a physical presence to deform overlying tissue, though some do mimic individual muscle actions.

2.4 Whole Body Modeling

The work that is closest to that presented in this paper is a system [Wil97], which we shall call the *ellipsoidal model*, that shows that simple animal models can be created and animated using only ellipsoidal approximations to underlying bones, muscles and generalized tissues. These elements are then covered by an implicit skin surface. The research described here differs from and extends that work in several ways:

1. Bones and generalized tissues can be triangle meshes, and muscles can be discretized deformable cylinders, whereas the ellipsoidal model requires all underlying components to be ellipsoids.
2. Muscles are closely based on the main muscles found in the body, whereas the ellipsoidal model just gives a general impression of shape.
3. The muscle model accommodates two pairs of attachments (i.e., two origin points and two insertion points, see Section 4 for terminology), located parametrically on individual bones, which is biologically more realistic than single attachments; the ellipsoidal model is inherently limited to single attachments.
4. Skin vertices are mapped to muscle space using a parametric trilinear mapping for smooth deformation in response to changes in muscle shape.
5. The final skin position is adjusted toward equilibrium, based on an elastic membrane model.
6. The skin surface extraction method permits finer resolution at the head and extremities, where details are most important, with a coarser resolution over the rest of the body.
7. The greater accuracy of this model makes it possible to see the effects of individual muscles on the skin, though the model is still very much an approximation compared to a real animal.

3 The Basic Model

Our body model uses a standard hierarchy of rigid segments connected by joints and emanating from a single root. The body consists of four types of materials. Individual *bones* are rigidly embedded in segments. Individual *muscles* are attached to bones, and stretch across one or more joints. *Generalized tissue* gives shape to regions where detailed bones and muscles aren't used, and for features such as eyes and nails. An elastic overlying triangle-mesh *skin* is attached to underlying tissues with anchors, but adjusts in response to forces from neighboring skin vertices. The model is appropriate for any vertebrate; we illustrate it here with a monkey body model.

The monkey model has 85 segments, including all segments connected by major moving joints in a vertebrate body: skull, jaw, 44 vertebrae,¹ pelvis, arms, legs, wrists, ankles, fingers, and toes. All joints are capable of three revolute degrees of freedom, but their range can be limited by a maximum and minimum angle. (Three translational degrees of freedom between segments are available, but not normally used.) Also, one can designate “synergies”, so that a requested rotation is distributed over a *series* of joints. E.g., a 12 degree rotation of the thoracic region is interpreted as a one degree rotation at each thoracic vertebra. This makes it possible to control many degrees of freedom easily, and has some basis in fact, because joints of the body do move as a group. We find synergies particularly useful for the spine and hands.

Figure 1 shows the underlying components and the skin in the rest position of the body. The rest position is represented in a geometry file. Each segment has a *basic segment size* based on this rest geometry, that is used in parameterizing components. The basic segment size is the long diagonal of a bounding box over the

¹7 cervical (neck), 13 thoracic (chest), 7 lumbar (lower back), 1 pelvis, 3 sacral, 13 caudal (tail).

segment defined by the positions of the segment origin and the origins of its child segments, defined in the local coordinate system of the segment. If a segment has no children, it uses the segment size of its parent. The use of the segment size in parameterization is described later.

3.1 Skeleton and Generalized Tissue

The skeleton and generalized tissues are modeled as triangle meshes or ellipsoids. Meshes should be closed polyhedra, so that there is a distinct inside and outside for voxelization. These components do not change shape during motion, but can change position relative to each other. Each has its own local coordinate system, which is positioned within a single body segment and moves with that segment. When stored, the sizes and locations of bones and generalized tissues are parameterized by the basic segment size. I.e., if a bone coordinate frame origin is located at (5,10,15) relative to its segment coordinate frame, and the basic segment size is 20, the bone origin is stored as (0.25,0.5,0.75). This way, the same components can be used in an individual where segments are different sizes.

The monkey skeleton consists of 88 individual triangle-mesh bones, which were originally taken from a human skeleton model from *Viewpoint DataLabs*, and altered using the *Alias/Wavefront* software to be more monkey-like. There are also 68 ellipsoidal bones for the tail and parts of the hands and feet. Bones are shown in white in Figure 1. All of the generalized tissue in the monkey model are ellipsoids, shown in purple in the lower left quadrant of Figure 1. There are 54 such ellipsoids in the monkey model. The eyes and nails are also modeled with ellipsoids.

4 Muscles

A typical skeletal muscle is an elastic, contractile material. In anatomical terminology it *originates* via tendons at fixed *origin* locations on one or more bones, passes across one or more joints, and *inserts* via tendons on fixed *insertion* locations on one or more other bones more distal to the body center. When the muscle contracts, and shortens, the bones to which the muscles are attached are pulled toward each other; usually the distal bone moves more than the proximal. The diameter and shape of the muscle changes depending on the relative positions of origins and insertions. In a real animal, muscle contraction causes joint motion. In our virtual animal, muscles change shape because of joint motion, to cause realistic skin deformations during animation.

Initial work [Wil97] used ellipsoids for muscles, which is adequate for those with a simple fusiform shape and a single origin and insertion. This model is insufficiently general for many muscles; e.g., only the lower arm muscles of the monkey model are ellipsoidal.

4.1 Deformed Cylinder Model for Muscles

Many muscles originate from or insert on more than one location. The various origins may be in different segments, and the same is true for insertions. To model such muscles, we have developed a muscle model based on a *deformed cylinder*. Our interests lie in producing relatively realistic animals that can be animated quickly and designed in a reasonable time frame. We have found this model to provide a good compromise between realism and speed.

Muscles may be sheet-like, and bend around other components. For example, the pectoralis major originates all along the breastbone (sternum) and is a relatively flat sheet that curves around the ribs and attaches to the upper arm (humerus). The triceps at the back of the upper arm has a tendon that stretches around the “funny bone” in the elbow and inserts on a lower arm bone (ulna).

An exact model of each individual muscle would be extremely complex and time-consuming, though a desirable long-term goal. As our interests lie in producing relatively realistic animals that can be animated quickly and designed in a reasonable time frame, we have chosen a muscle model based on a deformable cylinder.

The system generates, on request, a default deformed-cylinder muscle that is completely defined by two *origins* and two *insertions* (Figure 2). For example, the extended origin of the pectoralis is modeled by an origin at the top of the sternum and another at the bottom (Figure 3). Origin and insertion points are described as three-dimensional locations on specific bones, parameterized by the size of the bounding box of the bone. In this way, the same muscle model can be used in different individuals.

Origins and insertions may all be on different bones and in different segments. This flexibility is important for biological realism. There are two constraints on these four points. First, origins must be proximal relative to insertions in the body hierarchy (i.e., closer to the root of the hierarchy, in anatomical terminology). Second, the first origin listed in the specification file must be proximal to the second if they are on different segments; this just makes the programming slightly simpler.

Each muscle is a discretized, deformed cylinder whose axis is a curve that proceeds from the midpoint of the origins to the midpoint of the insertions. Generally, the cylinder is discretized into 7 longitudinal *muscle sections* demarcated by 8 elliptical cross-sectional *slices* (see Figs. 2 and 10). Though finer discretization can be used, this seems to provide a good approximation. A parametric trilinear function (more technically, a tri-affine function) is defined by adjacent slices, and is used to locate and move skin vertices (see Section 5.1).

The first elliptical slice lies between the two origins, and the last elliptical slice lies between the two insertions. The six intervening elliptical slices lie between and define the shape and longitudinal axis of the muscle. (The section of the muscle cylinder that begins at the origins, and the section that ends at the insertions, could be considered tendons, though they are not treated differently than the other sections in our model.) Each cross-sectional slice is then discretized into regularly spaced radial points, defining a planar polygon. Connecting the radial points between neighboring muscle cross-sections produces a polygon mesh. Figure 2 shows a default lower leg muscle in outline below and shaded above. Origins and insertions are shown as paired red and green spheres, and cross-sectional slices are shown in yellow.

While there are hundreds of individual muscles in the body, many are deep and small and have little external effect on shape. There are approximately 80 major muscles that affect the shape of the arms, legs, and trunk (ignoring fingers and toes), most of which occur symmetrically on the right and left sides of the body (i.e., there are about 40 on each side) [Wak79]. The monkey model used here groups some of these muscles, divides a few, and ignores others. 40 deformed-cylinder muscles are used altogether.

The basic muscle definitions are provided to the program by an ascii file giving the muscle name, its origin and insertion bones, and the parameterized two origin and two insertion locations for each muscle. This file was created manually, using texts on human and animal anatomy, which contain tables and diagrams describing this information. Origins and insertions can be interactively adjusted as needed for best effect, and the results saved.

When a muscle file is read, the origin and insertion bones are found and the externally stored *parametric* locations of the origin and insertion points are converted to *actual* locations in the local coordinate systems of appropriate bones. Remember that each bone's coordinate system is defined relative to the coordinate system of its segment. Origins and insertions are also internally stored relative to the segment coordinate frame. Origin and insertion locations are constant within their respective muscle, bone, and segment frames, so the calculation need only be done once.

4.2 Setting the Default Muscle Shape

The default muscle shape is automatically created based on the origins and insertions, and can then be altered interactively by the user. Figure 2 shows a default muscle, which illustrates the procedure described in this section.

There is a *slice* coordinate frame associated with each of the (normally eight) sliced segments of the muscle. The origins of these coordinate frames define the piecewise linear longitudinal axis of the muscle, and lie at the center of each slice ellipse. The X, Y, and Z axes of these slice frames are shown as red, green, and blue lines (respectively) in Figure 2. The XY planes of these slice coordinate frames define cross-sections of the muscle, and their Z-axis points along the longitudinal axis of the muscle, from muscle origins to muscle insertions. (We somewhat verbosely describe the (fixed) origin points of the muscle on bone as *muscle origins* and the origins of the slice coordinate frames as *coordinate frame origins* to prevent confusion in the different use of the word *origin*.)

The polyhedral vertices of the muscle's surface lie in the XY plane of each slice, arranged symmetrically around the slice coordinate frame origin, discretizing the ellipse. The number of vertices in each slice is under user control; the default number is 8. Figure 2 connects the muscle vertices within each slice with yellow lines, and muscle vertices between slices by reddish lines.

The locations of these frames and vertices are found as follows: First, all muscle origin and insertion locations are converted into the frame of the first muscle origin location's segment (i.e. the segment that contains the bone that the first muscle origin is attached to). The first muscle origin is just the one listed first in the muscle description file. Since the relative positions of muscle origins and insertions change during motion, this must be done anew each time any joint between origins and insertions changes.

Next, two end-slice coordinate frames are created. The midpoint of the two muscle origins becomes the origin of one end-slice frame, and the midpoint of the two insertions becomes the origin of the other. The lines between origins, and between insertions, define X-axes of end frames. (X-axes shown in red in the outline figures). The Z-axis of the origin slice coordinate frame is perpendicular to the X-axis and points outward from the origin bone. The Z-axis of the insertion slice frame is similarly perpendicular to the insertion frame X-axis, but points into the insertion bone. (Z-axes shown in blue in the outline figures.) These Z-axes are found by averaging the outward normal vectors to the bones at the origin locations, and the inward normal vectors to the bones at the insertion locations. The Y-axes for these coordinate frames (shown in green in the outline figures) complete right-handed systems.

Now, the planes of the intermediate slices are calculated. Initially, they are arranged along a straight line between the origins of the two end coordinate frames described above, and equidistant from each other along this line. The intermediate slice frames have their Z-axes aligned along the line between end coordinate frame origins, and their X-axes are interpolated between the X-axes of the end frames. Again, the Y-axes complete the right-handed systems. Once the thickness of the muscle slices is found, the origins of the intermediate frames are slightly displaced in the negative Y direction (outward from the underlying bone), to compensate for the greater thickness of the muscle near its center. Thus, the centers of the muscle follow a curved path from origin to insertions.

Finally, the vertices around each slice frame, which define the actual polygon mesh for the muscle surface, are calculated. These points are radially located around the coordinate frame origin of the slice in its XY-plane. They are stored in an ellipse around that origin. The two end coordinate frames are constrained so that the width of the muscle (in X) is the distance between muscle origin points, and muscle insertion points, respectively. The vertex locations for the intermediate slices are scaled in X and Y to produce a fusiform shape, larger in the middle slices than in the end slices, and larger across (in X) than in thickness (in Y).

The default muscle shape, while somewhat complex to describe in words, is easily found using standard transformation methods common in computer graphics.

4.3 Non-Default Muscle Shapes

Often, the default muscle shape is not the right thickness, or does not take into account underlying parts well. The user can interactively alter the size of a muscle, and the orientation and location of slice coordinate frames, and the locations of origins and insertions. Figure 3 shows two non-default muscle shapes (the pectoralis major and quadriceps femoris), which illustrate the topics of this section.

First, the interface provides a facility to change the scale factors defining the X-width and Y-thickness of a muscle or any individual muscle slice. The cross-section of the muscle is always elliptical, controlled by the X and Y scale factors, which are modifiable by the user. Because most muscles show a great deal of symmetry in their external cross-sections, this was deemed a reasonable simplification, and it makes muscle shape modification much easier than moving individual muscle vertices would be. It does mean that muscles internally may intersect other body components. Muscles such as the gastrocnemius in the leg, the biceps in the arm, and the sterno-cleido-mastoid in the neck are well represented by slightly scaling the default muscle shape.

Other muscle-modification parameters alter location and orientation of the muscle slice coordinate frames. The simplest modification is to interactively translate the coordinate frame origin of any slice from its default location. (This can only be done to the intermediate slices, because the end slices are constrained by the muscle origins and insertions.) This is used for muscles like the pectoralis, across the chest, which follows a curved path from the sternum, around the ribs, to the arm. The orientation of the slice frames can also be rotated, in X, Y, or Z for intermediate frames, or in X alone for end frames.

Figure 3.A shows the pectoralis major muscles in the chest as shaded polygons on the left and in outline on the right. Note that the shape of the muscle is more triangular than fusiform, the muscle is quite flat, and the slice coordinate frames are in an arc around the ribs, not in a straight line from origin to insertion.

Another modification method is to designate a *pivot* coordinate frame. In this case, the path of the muscle is not from muscle origins to insertions, but from origins to pivot, then from pivot to insertions. Pivots are helpful in modeling muscles that must bend over joints, such as the quadriceps femoris, which runs across the front of the thigh and bends over the knee (Figure 3.B). The origins of pivot coordinate frames are shown as blue spheres in outline figures. Generally, pivots can reduce the problem of interpenetration of the muscle with the material beneath it. (See Section 7 for further discussion of this problem.)

The pivot frame is defined relative to a specific segment, usually that of the segment containing the bone to which the first muscle origin is attached. Its location and orientation are under user control. A specific slice uses the pivot frame as its slice frame, and other frames arrange themselves on the line to the pivot frame, or from the pivot frame, depending on their position relative to the pivot slice. The pivot frame can be permanently in effect (always used), or it can be used intermittently depending on whether the joint

2 origin locations parameterized on bones (x,y,z)
2 insertion locations parameterized on bones (x,y,z)
x,y scale of each muscle shape slice
x,y,z translate of slice coordinate frame from default
x,y,z rotation of slice coordinate frame from default
whether pivot is on, off, or variable
which muscle shape slice acts as the pivot
location of the origin of the pivot coordinate frame
orientation of the pivot coordinate frame

Table 1: Muscle parameters controllable by the user.

angles make it natural to use it. In Figure 3.B, the pivot frame is the seventh frame, as the bend occurs near the very end of the muscle. The right leg is in its rest position, and the left lower leg is flexed, showing the muscle bending around its pivot.

Table 1 summarizes the user-controllable parameters for muscle design. Nearly all the muscles in the monkey model shown in Figure 1 used some non-default parameters.

4.4 Muscle Animation

Muscle animation involves the automatic recalculation of the muscle shape whenever a joint lying between muscle origins and insertions moves. The muscle origins and insertions are converted to the frame of the first origin, given the new joint positions. A default shape is found, and automatically adjusted using the user-specified non-default muscle parameters described in the previous section.

Finally, the muscle width and thickness are scaled to maintain approximately constant muscle volume during joint changes. The *rest length* of the muscle is the distance from the midpoint of the muscle origins, through the pivot, if present, to the midpoint of the insertions, while the muscle is in the resting position, as designed. A *present length* is similarly calculated for when the muscle is repositioned due to joint changes. The width and thickness of the internal slices of the muscle (not the end slices) are scaled by $\sqrt{\text{rest length} / \text{present length}}$. This increases the cross-sectional area if the muscle shortens, and decreases it if it lengthens. Volume is preserved exactly in regions between parallel slices, and is changed as a second order effect in regions between two nonparallel scaled slices. However, end slices do not change shape, so regions involving an end slice will normally vary in volume.

In any case, exact volume preservation of muscles is not biologically justified. Isometric deformations provide a case in point. Future work should address a more flexible and more biologically sophisticated method for adjusting muscle volume.

The new muscle shape is stored and reused for display and skin adjustment purposes until another joint change necessitating recalculation occurs. Figure 5 shows four stills from an animation of the shoulder muscles (shown in red outline) deforming during motion. Figure 4 shows a muscle from the front and side at three levels of contraction.

5 Skin

The skin is an elastic triangle-mesh surface that is attached to underlying components but can move relative to them; i.e., a separate, controllably loose layer over underlying components. The initial creation of the surface is based on fairly standard implicit surface techniques [WMW86, Blo88, WK94, Wil97], and is summarized below. The novel contribution of this paper is the methodology for skin deformation in response to deformation of the underlying tissue, described in subsequent subsections.

The region around the animal in the rest position is voxelized to create a three-dimensional discrete grid of points. Values at points define an artificial *density function* that is positive if the point is inside any body part and zero otherwise. (In addition, certain artificial components may have a *negative* density to create a repulsion effect, discussed below.) Then the initial density function is filtered with a Gaussian kernel, whose width is under user control. The user chooses a threshold, and an isosurface of the filtered density is extracted as a triangulated surface mesh.

Figure 6 shows these steps. Upper left shows the underlying components; the head and extremities are enlarged for better skin detail in those areas, as described in Section 5.3. Upper right is a voxel grid whose maximum resolution is 200, showing interior grid points in magenta. Grid points outside the body are not shown. Interior points are given a value of 200. Exterior points are given a value of 0. The purple spheres

near the eyes are actually *negative components*, which have a value of -100. Use of negative components drives the isosurface away from those regions, making deep orbits for the eyes to sit in. Lower left is the voxel grid after filtering, showing the grid points with positive field values in cyan. The Gaussian filter kernel had a standard deviation of about 3 voxel separations. Lower right is the extracted skin, with an isosurface value of 30.

5.1 Anchoring Skin

After surface extraction, in a second stage called *anchoring*, each vertex in the triangle-mesh skin is associated with the closest underlying body component (muscle, bone, or generalized tissue).

The *anchor* of a particular skin vertex is the nearest point on its underlying component. More important for animation is the *virtual anchor*, which is the initial position of a skin vertex relative to its underlying component. This is the position of the vertex when the skin was extracted, which is generally over body components that are in a rest position. The anchors and virtual anchors are stored parameterized in the local space of the component. If shape changes occur in the underlying component, they are transmitted through the anchors and virtual anchors, to affect the skin vertices correspondingly. Each skin vertex is considered to be connected to its virtual anchor by a spring of rest length zero, and a specified spring stiffness. Spring parameters are discussed in Section 5.2.

Anchoring refers to the process of finding the nearest underlying component of each skin vertex, converting that skin vertex to a parameterized local location relative to the component, and storing this local position of the skin vertex as its virtual anchor. Anchoring skin to ellipsoids was previously described [Wil97]. Anchoring skin to triangle-mesh bones is simple, because they don't change shape. The skin vertices are converted into the coordinate system of the bone and scaled by the size of its bounding box in each dimension. Anchoring points to deformed-cylinder muscles is a more interesting problem, and is now described.

A skin vertex is associated with a muscle if it is found to be closer to the polygonized surface of the muscle than to any other underlying component in the body. The skin vertex is then associated with a section of the muscle that lies between two muscle slices. I.e., if it is closest to a polygon stretching from slice 4 to slice 5, the skin vertex is associated with the segment between those slices. Figure 10 shows these concepts. The lighter skin vertex lies nearest to the muscle segment between slices 4 and 5, and will be mapped to a parametric location in this region. One cannot simply map the skin vertices into the frame of single slice, because bumps appear in the skin when the muscles change shape, due to the abrupt changes in mapping from one slice frame to the next.

Rather, we define a *parametric trilinear transformation* (more precisely named "tri-affine") over the space between the planes of the two slices in rest position, and assign parameters to the virtual anchor in accordance with the inverse of this transformation. A parametric trilinear transformation is a three-vector of independent trilinear functions, each of which maps parameter-space (s, t, u) into physical-space (X, Y, Z) .

$$\begin{aligned} X(s, t, u) &= A_x s + B_x t + C_x u + D_x st + E_x tu + F_x su + G_x stu + H_x \\ Y(s, t, u) &= A_y s + B_y t + C_y u + D_y st + E_y tu + F_y su + G_y stu + H_y \\ Z(s, t, u) &= A_z s + B_z t + C_z u + D_z st + E_z tu + F_z su + G_z stu + H_z \end{aligned}$$

The parametric trilinear transformation maps a unit cube into a warped cell such that edges in the original cell remain as straight lines. Parametric trilinear transformations are defined on adjacent cubes so that they map each shared corner of their cubes to the same point. This ensures that they combine to make a C^0 continuous transformation. Parametric trilinear transformations are often used in computational fluid

dynamics simulations to map regular grids into “warped” curvilinear grids. Related ideas are found in free-form deformations of computer modeling [SP86], but usually higher-order functions are used. We do not need the higher orders of continuity because this mapping is only used to give an initial skin position, which is then adjusted towards elastic equilibrium (see Section 5.2).

The parametric trilinear transformation for a muscle segment is found by taking four corresponding muscle vertices from each of the slice planes that bound the segment. The four from the “proximal” slice will be the image of a parametric unit cube’s $u = 0$ face, while the four from the “distal” slice will be the image of the unit cube’s $u = 1$ face. Joining corresponding vertices of the two slices makes the warped image of the unit cube. In Figure 10 such a warped cell is shown in red. These eight vertices provide the 24 unknowns necessary to specify the coefficients of the parametric trilinear transformation. Each skin vertex associated with a particular muscle segment is then mapped inversely to a parametric position (s, t, u) within the domain of the parametric trilinear transformation defining that segment. The inverse mapping has no closed form, and requires 3D Newton-Raphson iteration [VGW92]. The (s, t, u) parameterized position is the virtual anchor for that skin vertex. This expensive operation needs to be done only once per point, during anchoring.

Now we describe how the (s, t, u) parametric position is used. When the body is moved, new world space positions are calculated for the slices (see Section 4.4). Then for each adjacent pair of slices a *new* parametric trilinear transformation is defined. (This process is not expensive, compared to calculating general inverse mappings.) Virtual anchor points associated with this segment are mapped from (s, t, u) to world space, using the new parametric trilinear transformation, in the *forward* direction. Each virtual anchor provides an initial skin position for its corresponding skin vertex, for this body configuration.

Figure 7 illustrates these concepts on the left shoulder and arm of the monkey. The arm is raised away from the rest position, with consequent deformation of nearby muscles. In the left image, virtual anchor points have been remapped from parameter space to world space, taking into account both the rigid motion and deformation of their respective muscles, but no elastic relaxation has been done. The yellow lines connect skin vertices to their muscle anchors, i.e., their closest underlying component when they were extracted in a rest state. Magenta lines connect skin vertices to anchors on bones. At this point, the skin vertices and their virtual anchors are in the same position. This initial position is generally undesirable, because skin vertices attached to components on opposite sides of a moving joint can be pulled very far apart or pushed into each other, as is obvious from Figure 7. In world space, skin positions are now moved to achieve an elastic equilibrium, as described in Section 5.2, and shown in the right image of the figure.

5.2 The Elastic Model

The skin surface is defined as a triangle mesh. To simulate an elastic membrane each edge of the triangle mesh is considered to be a spring with a certain rest length and stiffness. Together with other forces and constraints in the system, these springs are brought into equilibrium by means of a series of relaxation operations. The initial skin positions, from which relaxation commences, are provided by the positions of the virtual anchor, as described in Section 5.1. Relaxation operations continue iteratively until a user-defined convergence tolerance is reached, or a user-defined maximum number of iterations has occurred. Details of the spring forces and other constraints are now described.

The spring stiffness coefficient (stiffness, for short), for edges between skin vertices is denoted as k_e . This value is automatically calculated as

$$k_e(v, v_j) = \frac{a_1 + a_2}{len^2} \quad (1)$$

where len is the length of the edge between skin vertices v and v_j , and a_1 and a_2 are the areas of the two

triangles sharing the edge, all calculated once in the rest position. This formula provides a more accurate model of uniformly elastic skin than would uniform stiffness for all springs [VGW97b]. The formula used is simplified from the general case by assuming the Poisson coefficient for skin is 0. (A more complicated formula with the more realistic Poisson coefficient of 0.25 did not produce observable differences.) Variations in elastic properties can be defined by the user, if desired.

The spring stiffness for the edge between the skin vertex and its virtual anchor is denoted as k_a . This “edge” has zero rest length. For each skin triangle, the force resulting from pulling the skin away from the underlying material is assumed to be proportional to the area of the triangle (as is standard for “body forces” in elasticity), and this area is distributed equally to the three skin vertices incident upon the triangle. Consequently,

$$k_a(v) = \frac{C_a \sum_i a_i}{3} \quad (2)$$

where a_i denotes the area of the i -th triangle incident upon the skin vertex v , and the sum is over all such triangles. The coefficient C_a is a proportionality constant to control the relative strengths of skin-skin springs (k_e ’s) and skin-virtual-anchor springs (k_a ’s). For the monkey model, the anchor spring stiffness is generally scaled by $C_a = 0.10$, which allows the skin to slide readily over the underlying parts. If constant spring stiffness coefficients are used instead of the geometrically determined values in Eqs. 1–2), then we observed that the equilibrium position of the skin appears irregularly stretched.

To find the change in position to be applied to a vertex due to the influence of a connected edge, the elastic force vector is calculated. First, the vector $w_j = v_j - v$ is defined, where v is the vertex being analyzed, and v_j is the vertex at the far end of the edge. The length of w_j is the present length of the edge. The rest length of the edge is subtracted from the present length, giving the *length excess*, which may be negative. Now the spring stiffness, $k_e(v, v_j)$ may be modified, based on the *length excess*, providing a form of nonlinear spring (see below). The *length excess* is multiplied by the (possibly modified) spring stiffness for the edge to give the scalar value of elastic force due to this edge. The direction of the elastic force is just the direction of w_j . Thus the elastic force is toward v_j if the *length excess* is positive, and away from v_j if it is negative.

For each vertex v , the sum of the elastic forces due to each of its edges to other skin vertices v_j , and due to the edge to its virtual anchor, defines the *net elastic force* acting on this vertex. This net force is divided by the sum of the spring stiffness coefficients that contributed to the net force, giving the *elastic relaxation vector* for v . (This denominator is conservatively large, as various forces tend to cancel each other; however it stabilizes the relaxation.) All skin vertex positions are translated by their relaxation vectors in one round of relaxation. The relaxations are iterated until the maximum relaxation vector is below the user-specified threshold, or the user-specified maximum number of iterations occurs.

Figures 8 and 9 show the effect of elastic relaxation on the skin. In the left images, skin vertices have not been adjusted, and lie on their virtual anchors. In the right images, thirty iterations of relaxation have been applied. In Figure 8, the texture indicates the shape of the skin triangles relative to their rest shapes. In the rest position, all dots are circular and fit within a particular triangle. Since the isosurface extraction produces triangles of varying size and shape, the circles are of different sizes. Notice that after iteration, most of the dots are deformed about equally from their initial circular form. In Figure 9, the fur attached to skin triangles is pulled apart and the skin is stretched abnormally in the left, non-relaxed image, but both appear normal in the right image [VGW97a].

A few other parameters can be applied to the skin. First, we want the skin to *pull* from a stretched position toward its rest state more strongly than it *pushes* back when it is compressed. Therefore, a user-controlled scale factor can be applied to scale down the spring force if the present length is less than the rest length. Typically this scale factor is 0.1.

Second, the skin can appear more smooth if we adjust the model so that the skin is slightly stretched in its extracted configuration. I.e., the *rest length* of the edge is taken to be some percentage of the measured *default length* of the edge when extracted. Suppose the user has chosen 90% for this parameter, and 0.1 for the above “pushing back” parameter. Then k_e , the spring stiffness will be modified by the following continuous function of *length excess*, discussed above. If *length excess* is positive, k_e is used as is (100%). If *length excess* is more negative than $-0.1 \times (\text{rest length})$, then $0.1k_e$ is used (10%). If *length excess* is between these bounds, the multiplier for k_e is interpolated between 10% and 100%. We believe that this continuous transition of stiffness also serves to stabilize the relaxation process, but do not have definite data to support our belief.

Finally, a collision influence can be applied to prevent the skin from sinking into underlying components. Each skin vertex is prohibited from penetrating a sphere whose center is somewhat below the anchor point in the underlying component. The surface of this sphere is tangent to the tangent plane of the skin at the virtual anchor point. I.e., if the calculated new position of the skin vertex penetrates such a sphere, a repelling force is activated to displace the skin vertex outward toward the sphere surface.

This approach only handles collisions between the skin and its nearby underlining tissues. A second collision type occurs when a joint is bent so that skin on either side of the joint meet. In this case interpenetration can occur, but it is hidden within the folds of the skin. A third collision type occurs when skin from one part of the body presses on another. This would require modeling the influence of external collision forces on the skin, which we do not do.

5.3 Non-Uniform Scaling and Re-usability

Because all components are parameterized, they can be re-used to a large extent in different individuals. The basic reference for all components is ultimately the basic segment size, calculated as described in Section 3 from the rest geometry of the animal. If a model with larger or smaller segments is used, components compensate automatically for the change in size.

For easy scaling, it is possible to scale the basic size by applying an extra scale factor to each segment when the body is read in. In this way, we created the model shown in Figure 6, with extra large extremities. By voxelizing such a model, more detail is preserved in the hands and feet. The skin is then saved, and can be re-used on a model with more normal-sized segments. All the monkeys shown in this paper used such scaling. Because of the similarity between vertebrates, many of the components of one model can be used for other species as well. It is also possible to scale the thickness of the skin, by moving the virtual anchors further from their underlying components.

Figure 11 shows the effects of scaling. These three monkeys were made from the identical underlying components and skin as all the other monkeys in the paper but in the left image the arms are lengthened, in the right image the legs are lengthened, and in the center the skin thickness is increased to create a plump monkey.

6 Results and Discussion

As mentioned above, the monkey model contains 85 body segments, 156 bones, 52 muscles, and 54 generalized components. The skin was voxelized over a grid whose maximum dimension was 225. Internal points were assigned 200 as density, outside points were 0. It was filtered by a Gaussian kernel with standard deviation 3.2. The isosurface threshold was 35. There are about 75,000 skin vertices and about 150,000 skin triangles. Table 2 gives times for various steps.

Steps Done Once to Create Skin	
Voxelization (Max. Dim. 225)	185
Filtering (3.2 std.dev. kernel)	160
Isosurface Extraction	16
Anchoring	645
Steps Required if Joints Moved	
Redraw of Underlying Components	Less than 1
Skin Repositioning - 0 relaxations	3
Skin Repositioning - 10 relaxations	9
Skin Repositioning - 30 relaxations	25

Table 2: Elapsed times in seconds for various steps, on an SGI with four 150-MHz R4400 processors, using shared-memory multi-processing.

Figure 12 shows a selection of monkey images in various positions. The “mohawk” fur [VGW97a] is a rather whimsical addition to make the monkey seem less bald without obscuring the skin deformations that we wish to emphasize.

The parameterized muscle shape model is fast and easy to change, and provides a good approximation to the shape of most muscles (but see below). The monkey model could be improved by making more muscles. There can be problems in certain extreme positions. However, as the images and animations show, the body looks good over a wide range of motions.

The most time-consuming part of creating the model was to model individual muscles. Knowledge of anatomy is helpful, although students with no background in anatomy were able to perform many modeling tasks with light supervision of a trained biologist, and appropriate texts on anatomy (e.g., [Wak79]).

An alternative to adjusting a permanent skin in response to underlying tissue deformations would be to re-extract skin over new body positions. However, this would raise questions about consistency from one position to the next. For example, how would a texture be associated with the skin that appears to shift realistically?

The current skin model produces a smooth surface that is visually close to equilibrium after about 30 iterations; after this, changes from one iteration to the next are barely noticeable. Even after 5 or 10 iterations, acceptable convergence is found in many cases.

7 Future Work

This remains a very approximate model when compared to actual animal anatomy. It is a reasonable compromise between detailed realism and acceptable modeling and animation speed, and is a considerable step forward from ellipsoidal models.

The major next step we envision is underlying components that interact with each other, and do not interpenetrate. This will allow more detailed, space-filling components to be created, which reposition themselves based on influences from neighboring components. Generalized tissue should also be extended to accommodate shape changes, as muscles do now. While these additions will be more expensive, the minimal computational cost of adjusting the present underlying components suggest it will still be feasible in a fairly interactive system.

It would be a relatively simple matter to have muscles pull on their bones and implement a real physically based simulation of joint motion. This could be useful for educational purposes or for research

in biomechanics. However, the control problems of physically simulating general realistic motion using contraction of individual muscles is really beyond present capabilities.

It would be desirable to have more detail in the face than provided by the non-uniform scaling. Because the skin is initially a separate polygonal layer that is then connected to the underlying components, it would be possible to connect a triangle-mesh skin from elsewhere to underlying components. For example, a digitized head model or a model extracted from CT scans could be connected to the underlying parts. This would require appropriate positioning and scaling. The skin and underlying components should also react to outside forces, such as gravity, and detect and respond to all collision types.

8 Conclusions

This paper describes a new and improved modeling and animation approach for animals and humans that is based on actual three-dimensional representations of individual body components such as bones, muscles, and miscellaneous tissue, covered by a skin. We believe this is the most natural approach to use for creating realistic animals and humans. The scheme is a good compromise between realism and complexity, and can be displayed and animated interactively. We believe the approach can be extended to produce much greater realism at an acceptable computational cost.

Acknowledgments

List processing software by Yumi Tsuji was used in this software package. Marlon Veal helped with programming. Research supported by a gift from Research and Development Laboratories, and by NSF Grant CDA-9115268.

References

- [Bar84] Alan H. Barr. Global and local deformations of solid primitives. In Hank Christiansen, editor, *Computer Graphics (SIGGRAPH '84 Proceedings)*, volume 18, pages 21–30, July 1984.
- [Bli82] James F. Blinn. A Generalization of Algebraic Surface Drawing. *ACM Transactions on Graphics*, 1(3):235–256, July 1982.
- [Blo88] Jules Bloomenthal. Polygonization of implicit surfaces. *Computer-Aided Geometric Design*, 5:341–355, 1988.
- [BOT79] Norman I. Badler, Joseph O'Rourke, and Hasida Toltzis. A spherical representation of a human body for visualizing movement. *Proceedings of the IEEE*, 67(10):1397–1403, October 1979.
- [BPW93] Norman I. Badler, Cary B. Phillips, and Bonnie Lynn Webber. *Simulating humans : computer graphics animation and control*. Oxford University Press, New York, 1993.
- [BZ91] Norman Badler and David Zeltzer, editors. *Making Them Move*. Morgan Kaufmann Publishers, Inc., San Mateo, CA., 1991.
- [Car94] Phil Carpenter. Commercial spot cola bears. *Cinefex Magazine*, December 1994.
- [Cat72] Ed Catmull. A system for computer-generated movies. In *Proceedings of the ACM Annual Conference*, pages 422–431. ACM, 1972.

- [CHP89] John E. Chadwick, David R. Haumann, and Richard E. Parent. Layered construction for deformable animated characters. *Computer Graphics (ACM SIGGRAPH Proceedings)*, 23(3):243–252, August 1989.
- [CZ92] David T. Chen and David Zeltzer. Pump it up: Computer animation based model of muscle using the finite element method. *Computer Graphics (ACM SIGGRAPH Proceedings)*, 26(2):89–98, July 1992.
- [dFdMGTV92] L. H. de Figueiredo, J. de Miranda Gomes, D. Terzopoulos, and L. Velho. Physically based methods for polygonization of implicit surfaces. In *Proceedings of Graphics Interface '92*, pages 250–257, May 1992.
- [DG95] Mathieu Desbrun and Marie-Paul Gascuel. Animating soft substances with implicit surfaces. *Computer Graphics (ACM SIGGRAPH Proceedings)*, pages 287–290, August 1995.
- [DL95] Scott L. Delp and J. Peter Loan. A Graphics-based Software System to Develop and Analyze Models of Musculoskeletal Structures. *Computers in Biology and Medicine*, 25(1):21–34, 1995.
- [FB88] David R. Forsey and Richard H. Bartels. Hierarchical b-spline refinement. *SIGGRAPH '88 Conference Proceedings*, 22(4):205–212, August, 1988.
- [Gas89] Marie-Paule Gascuel. Welding and pinching spline surfaces: New methods for interactive creation of complex objects and automatic fleshing of skeletons. In *Graphics Interface '89 Proceedings*, pages 20–27, June 1989.
- [GMTT89] Jean-Paul Gourret, Nadia Magnenat-Thalmann, and Daniel Thalmann. Simulation of object and human skin deformations in a grasping task. *Computer Graphics (ACM Siggraph Proceedings)*, 23(3):21–30, July 1989.
- [HDD⁺93] Hugues Hoppe, Tony DeRose, Tom Duchamp, John McDonald, and Werner Stuetzle. Mesh optimization. *Proceedings of SIGGRAPH*, 25(2):19–25, August 1993.
- [HE78] Don Herbison-Evans. Nudes 2: A numeric utility displaying ellipsoid solids. *SIGGRAPH '78 Conference Proceedings*, pages 354–356, August, 1978.
- [Hen90] Mark Henne. A Constraint-Based Skin Model for Human Figure Animation. Master's thesis, University of California, Santa Cruz, Santa Cruz, CA 95064, June 1990.
- [HHS87] M. Hahas, H. Huitric, and M. Saintourens. Animation of a b-spline figure. *The Visual Computer*, 3(4), 1987.
- [KCP92] James R. Kent, Wayne E. Carlson, and Richard E. Parent. Shape transformation for polyhedral objects. *Computer Graphics (ACM SIGGRAPH Proceedings)*, 26(2):47–54, July 1992.
- [KGC⁺96] R. M. Koch, M. H. Gross, F. R. Carls, D. F. von Buerin, G. Fankhauser, and Y. I. H. Parish. Simulating facial surgery using finite element models. *Computer Graphics (ACM SIGGRAPH Proceedings)*, pages 421–428, August 1996.
- [Kom88] K. Komatsu. Human Skin Model Capable of Natural Shape Variation. *The Visual Computer*, 4(3):265–271, 1988.
- [KWT88] Michael Kass, Andrew Witkin, and Demetri Terzopoulos. Snakes: Active contour models. *International Journal of Computer Vision*, pages 321–331, 1988.
- [LC87] William E. Lorensen and Harvey E. Cline. Marching cubes: A high resolution 3D surface construction algorithm. *Computer Graphics (ACM Siggraph Proceedings)*, 21(4):163–169, July 1987.

- [LTW95] Yuencheng Lee, Demetri Terzopoulos, and Keith Waters. Realistic modeling for facial animation. *Computer Graphics (ACM SIGGRAPH Proceedings)*, pages 55–62, August 1995.
- [MBL⁺91] James V. Miller, David E. Breen, William E. Lorensen, Robert M. O’Bara, and Michael J. Wozny. Geometrically deformed models: A method for extracting closed geometric models from volume data. *Computer Graphics (Acm Siggraph Proceedings)*, 25(4):217–226, July 1991.
- [Mil88] Gavin Miller. From wire-frames to furry animals. In *Graphics Interface ’88*, pages 138–145, Edmonton, Alberta, June 1988.
- [MN88] Don P. Mitchell and Arun N. Netravali. Reconstruction filters in computer graphics. *Computer Graphics (ACM Siggraph Proceedings)*, 22(4):221–228, August 1988.
- [MTT91] Nadia Magnenat-Thalmann and Daniel Thalmann. Human Body Deformations Using Joint-Dependent Local Operators and Finite Element Theory. In N. Badler, B. Barsky, and D. Zeltzer, editors, *Making Them Move*, pages 243–262. Morgan Kaufmann Publishers, Inc., San Mateo, CA, 1991.
- [MTT93] Nadia Magnenat-Thalmann and Daniel Thalmann, editors. *Models and Techniques in Computer Animation*. Springer-Verlag, New York, 1993.
- [Par82] Frederic Parke. Parameterized models for facial animation. *IEEE Computer Graphics and Applications*, 2(9):61–68, November, 1982.
- [PB81] Stephen M. Platt and Norman I. Badler. Animating facial expressions. *SIGGRAPH ’81 Conference Proceedings*, 15(3):245–252, August, 1981.
- [PB88] John C. Platt and Alan H. Barr. Constraint methods for flexible models. *Computer Graphics (SIGGRAPH ’88 Proceedings)*, 22(4):279–288, August, 1988.
- [SBD86] Francis J. M. Schmitt, Brian A. Barsky, and Wen-Hui Du. An adaptive subdivision method for surface-fitting from sampled data. *Computer Graphics (ACM Siggraph Proceedings)*, 20(4):179–188, August 1986.
- [SD93] Don Shay and Jody Duncan. *The Making of Jurassic Park*. Ballantine Books, New York, 1993.
- [SOP95] Karansher Singh, Jun Ohya, and Richard Parent. Human figure synthesis and animation for virtual space teleconferencing. In *Proceedings of the Virtual Reality Annual International Symposium ’95*, pages 118–126, Research Triangle Park, N.C., March 1995. IEEE Computer Society Press.
- [SP86] Thomas W. Sederberg and Scott R. Parry. Free-form deformation of solid geometric models. *Computer Graphics (ACM Siggraph Proceedings)*, 20(4):151–160, August 1986.
- [SPCM97] Ferdi Scheepers, Richard E. Parent, Wayne E. Carlson, and Stephen F. May. Anatomy-based modeling of the human musculature. *Computer Graphics (ACM Siggraph Proceedings)*, August 1997. To appear.
- [ST92] Richard Szeliski and David Tonnesen. Surface modeling with oriented particle systems. *Computer Graphics (ACM SIGGRAPH Proceedings)*, 26(2):185–194, July 1992.
- [SZL92] Williams J. Schroeder, Jonathan A. Zarge, and William E. Lorensen. Decimation of triangle meshes. *Computer Graphics (ACM Siggraph Proceedings)*, 24(2):65–70, July 1992.
- [TF88] Demetri Terzopoulos and Kurt Fleischer. Modeling inelastic deformation: Viscoelasticity, plasticity, fracture. *SIGGRAPH ’88 Conference Proceedings*, 22(4):269–278, August, 1988.
- [TPBF87] Demetri Terzopoulos, John Platt, Alan H. Barr, and Kurt Fleischer. Elastically deformable models. *SIGGRAPH ’87 Conference Proceedings*, 21(4):214, July 1987.

- [TT93] R. Turner and D. Thalmann. The Elastic Surface Layer Model for Animated Character Construction. In N. M. Thalmann and D. Thalmann, editors, *Proceedings of Computer Graphics International '93*, pages 399–412, Lausanne, Switzerland, June 1993. Springer-Verlag.
- [TT94] Xiaoyuan Tu and Demetri Terzopoulos. Artificial fishes: Physics, locomotion, perception, behavior. *Computer Graphics (ACM Siggraph Proceedings)*, pages 43–50, July 1994.
- [Tur92] Greg Turk. Re-tiling polygonal surfaces. *Computer Graphics (ACM SIGGRAPH Proceedings)*, 26(4):55–64, July 1992.
- [TW88] Demetri Terzopoulos and Andrew Witkin. Physically based models with rigid and deformable components. *IEEE Computer Graphics and Applications*, 8(6):41–51, November 1988.
- [TW90] D. Terzopoulos and K. Waters. Physically-based facial modelling, analysis, and animation. *The Journal of Visualization and Computer Animation*, 1(2):73–80, 1990.
- [TW93] Demetri Terzopoulos and Keith Waters. Analysis and Synthesis of Facial Image Sequences Using Physical and Anatomical Models. *IEEE Transactions on Pattern Analysis and Machine Intelligence*, 15(6):569–579, June 1993.
- [VGW92] Allen Van Gelder and Jane Wilhelms. Interactive Animated Visualization of Flow Fields. In *1992 Workshop on Volume Visualization*, pages 47–54, Boston, Mass., October 1992. ACM.
- [VGW97a] Allen Van Gelder and Jane Wilhelms. An Interactive Fur Modeling Technique. In *Proceedings of Graphics Interface*, May 1997.
- [VGW97b] Allen Van Gelder and Jane Wilhelms. Simulation of Elastic Membranes and Soft Tissue with Triangulated Spring Meshes. Technical Report UCSC-CRL-97-12, CS Dept., University of California, 225 A.S., Santa Cruz, CA 95064, January 1997.
- [Wak79] Marvalee H. Wake, editor. *Hyman's Comparative Vertebrate Anatomy*. University of Chicago Press, Chicago, Illinois, third edition edition, 1979.
- [Wat87] Keith Waters. A muscle model for animating three-dimensional facial expression. *SIGGRAPH '87 Conference Proceedings*, 21(4):17–24, July, 1987.
- [WH94] Andrew Witkin and Paul Heckbert. Using particles to sample and control implicit surfaces. *Computer Graphics (ACM SIGGRAPH Proceedings)*, pages 269–277, July 1994.
- [Wil97] Jane Wilhelms. Animals with Anatomy. *IEEE Computer Graphics and Applications*, 17(3):22–30, May 1997.
- [WK94] Sidney W. Wang and Arie E. Kaufman. Volume-sampled 3d modeling. *Computer Graphics and Applications*, 14(5):26–32, September 1994.
- [WKT96] Yin Wu, P. Kalra, and N. M. Thalmann. Simulation of Static and Dynamic Wrinkles of Skin. In *Proceedings of Computer Animation '96*, pages 90–97, Geneva, Switzerland, June 3–4 1996. IEEE Computer Society Press.
- [WMW86] Brian Wyvill, Craig McPheeters, and Geoff Wyvill. Animating soft objects. *Visual Computer*, 2:235–242, 1986.
- [WVG97] Jane Wilhelms and Allen Van Gelder. Anatomically based modeling. In *Computer Graphics (ACM SIGGRAPH Proceedings)*, Aug. 1997.

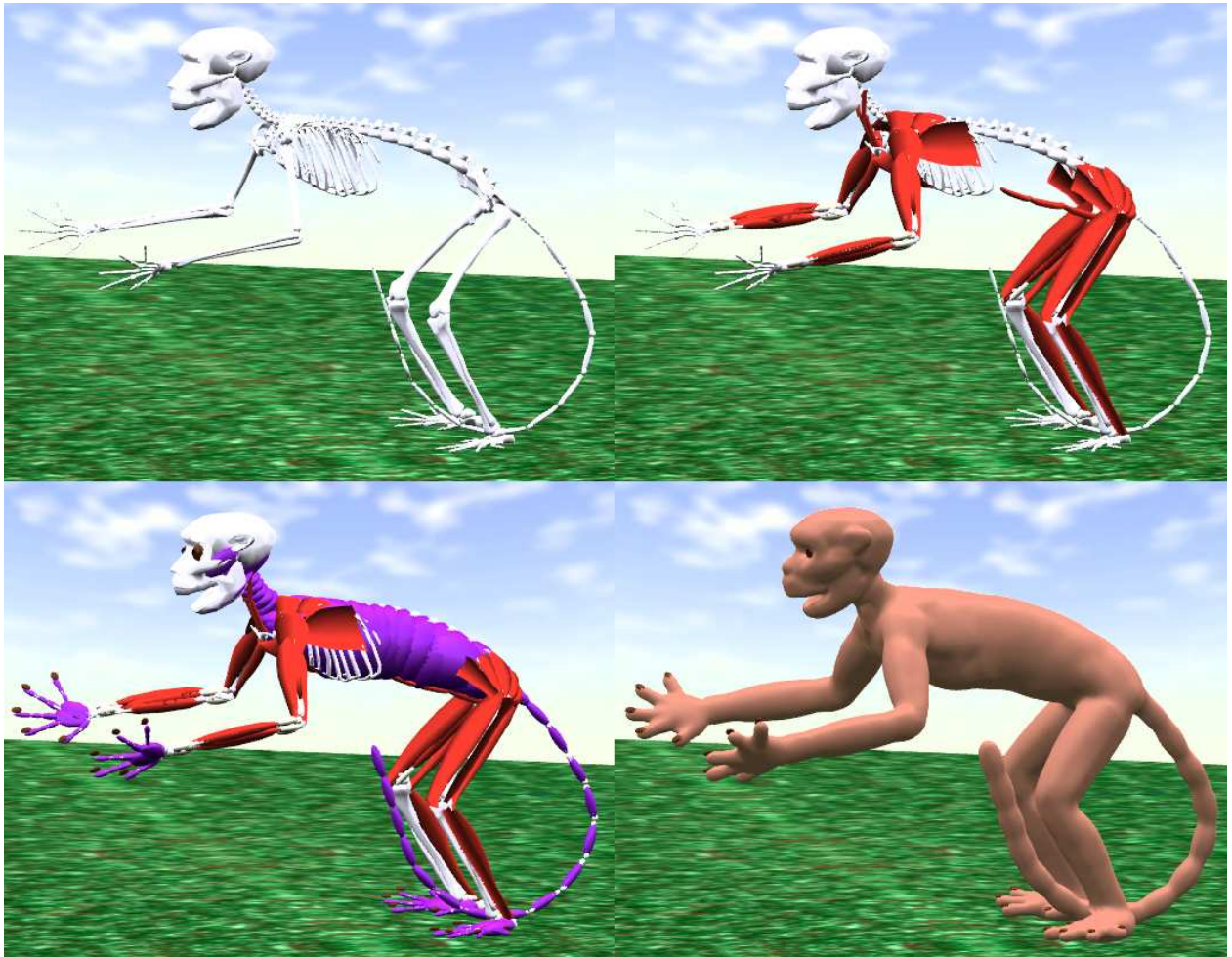


Figure 1: Anatomical components in the default resting posture. The skeleton is shown in white, the muscles in red, and the generalized tissue in purple. The skin with external features (eyes and nails) is shown in the lower right.

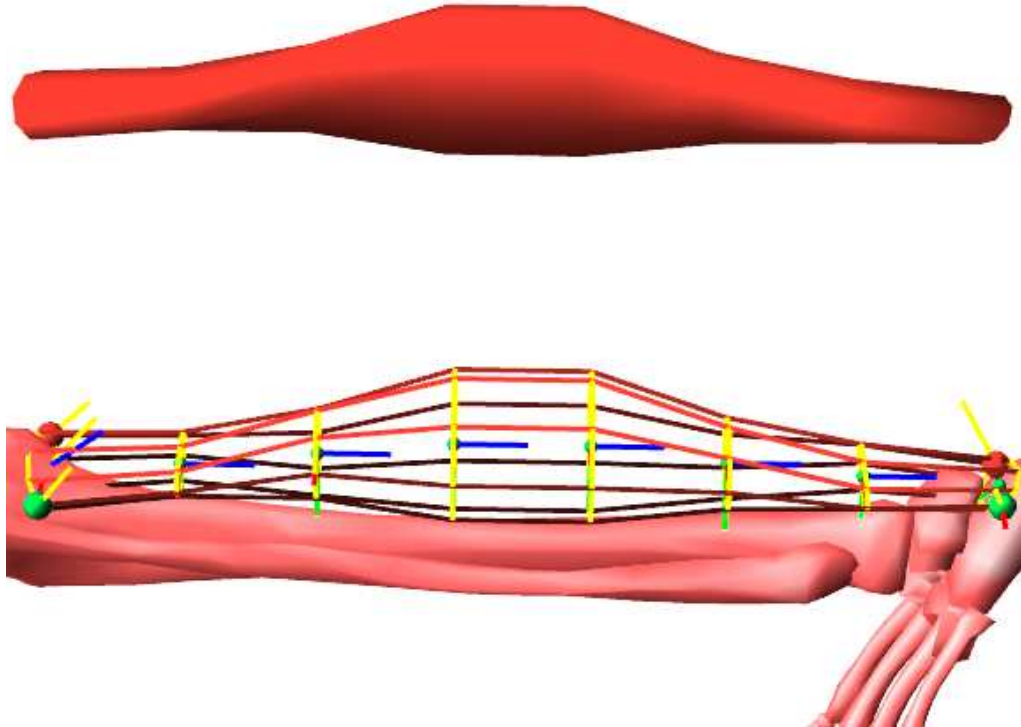


Figure 2: Typical default *deformed-cylinder* muscle, also illustrating anatomical terminology. The *proximal* direction is left, *distal* is right. The muscle is defined by two *origins* (red and green spheres at left) and two *insertions* (same at right). In the wireframe view below, eight yellow cross-sectional slices are connected by red edges to form a polygon mesh. The short blue and green lines are slice coordinate frame Z - and Y -axes. Note how the Z -axes rise from the origin bone at the first (left) slice, continue along the longitudinal axis of the muscle, and bend down into the insertion bone at the 8th (rightmost) slice. The shaded polygon mesh is shown above.

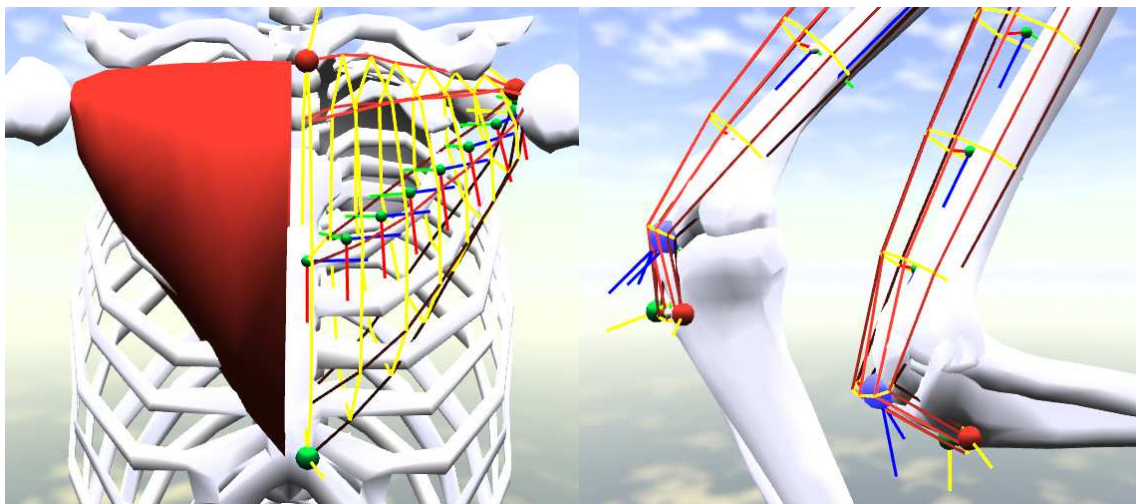


Figure 3: A. (at left) The right pectoralis major muscle, shown shaded, and the left, shown in outline, illustrate a non-default muscle shape set interactively by the user. B. (at right) The quadriceps femoris muscles illustrating the use of a pivot. The right lower leg is in the rest position, and the left lower leg is flexed showing the muscle bending around its pivot.

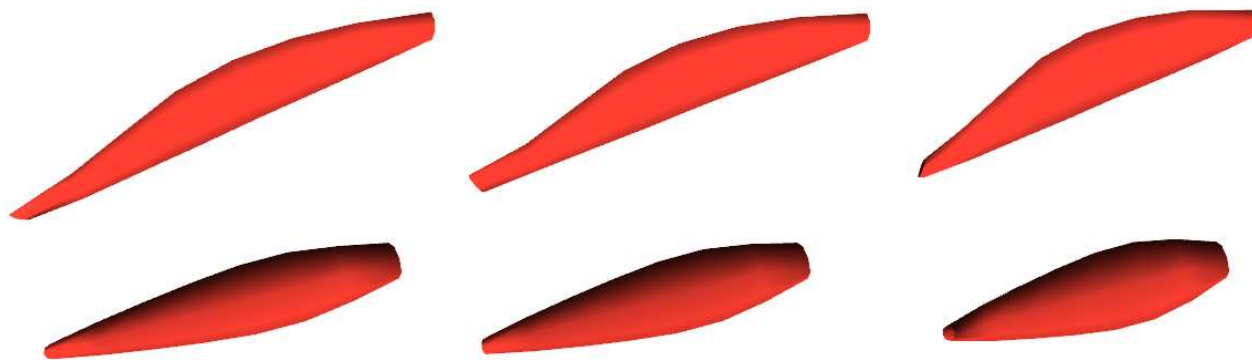


Figure 4: A muscle seen from side and in front at three different levels of contraction.



Figure 5: Four images showing shoulder muscle deformations (shown in red outline) during motion.

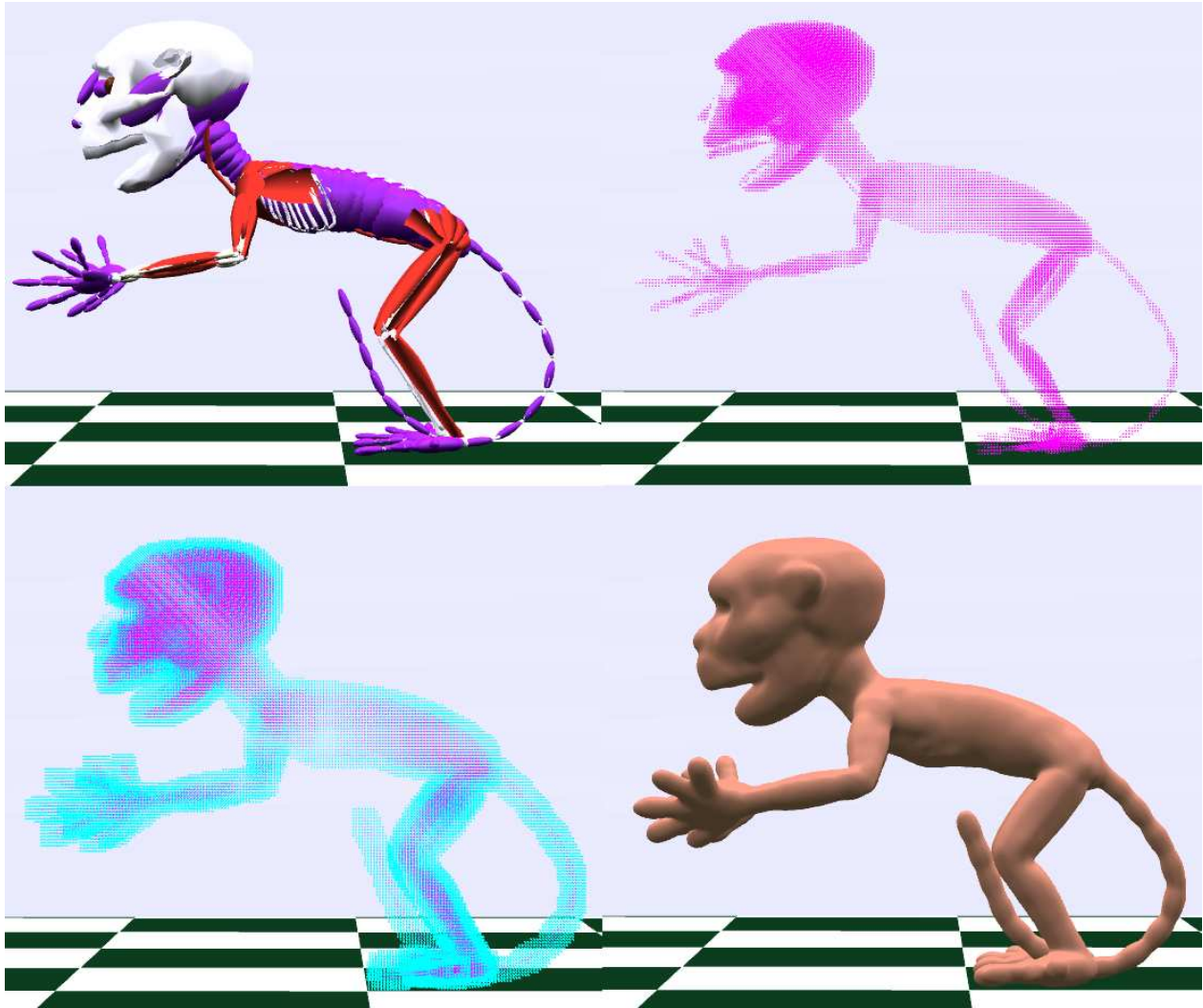


Figure 6: Voxelization and skin extraction illustrated: Upper left is the monkey with enlarged head and extremities for increased skin detail in those areas. Upper right is the initial “density” function over voxel grid whose maximum resolution is 200, showing positive densities in magenta. Interior points are given a value of 200. Exterior points are given a value of 0. Lower left is the “density” after filtering, showing grid points with positive densities in cyan. Lower right is the extracted skin, with an isosurface value of 30. Refer to Section 5 for further discussion.



Figure 7: This figure illustrates the concepts of anchors, virtual anchors, and elastic relaxations, on a raised left arm and shoulder. In the left image, skin vertices have been mapped from the positions of their virtual anchors into world space but no elastic relaxation has been done. The yellow lines connect skin vertices to their muscle anchors; magenta lines connect skin vertices to anchors on bones. At this point, the skin vertices and their virtual anchors are in the same position. In the right image, elastic relaxation has occurred and skin points are close to an equilibrium state. In this image, the red lines connect the skin vertices in their adjusted positions to their virtual anchors, showing the displacement necessary to equalize spring forces.

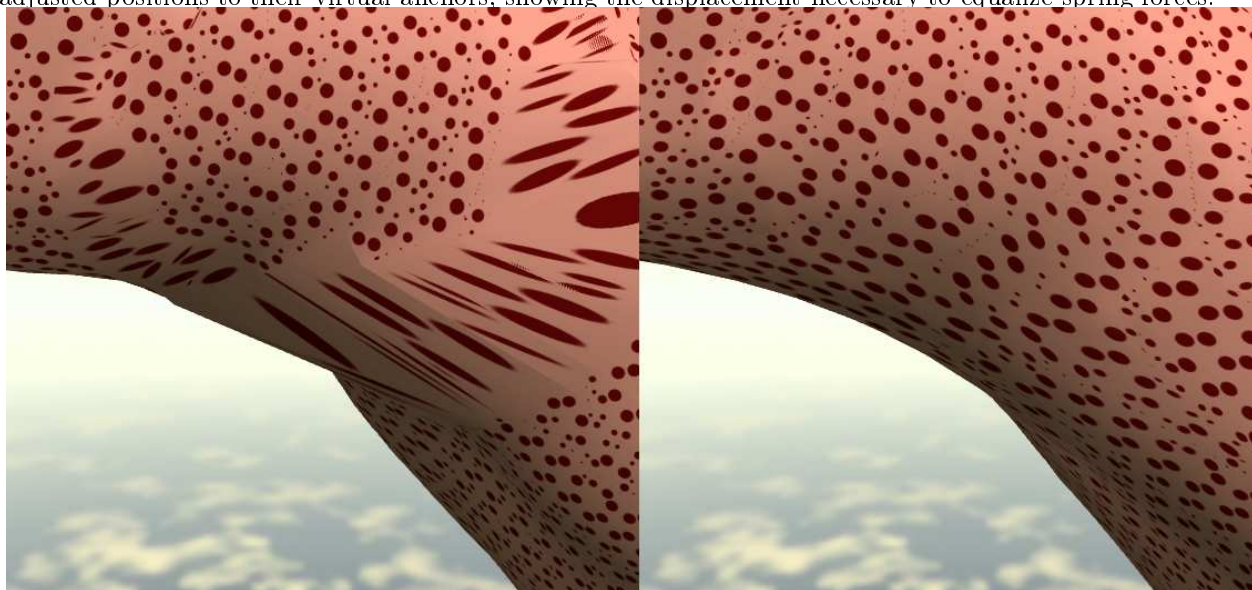


Figure 8: This figure illustrates the effect on skin of elastic relaxation, using the same model and position as in Figure 7. In the rest position, all dots are circular. In the left image, no elastic relaxation has occurred and skin vertices lie on their virtual anchors. In the right image, 30 relaxations have occurred and the skin has largely stabilized.

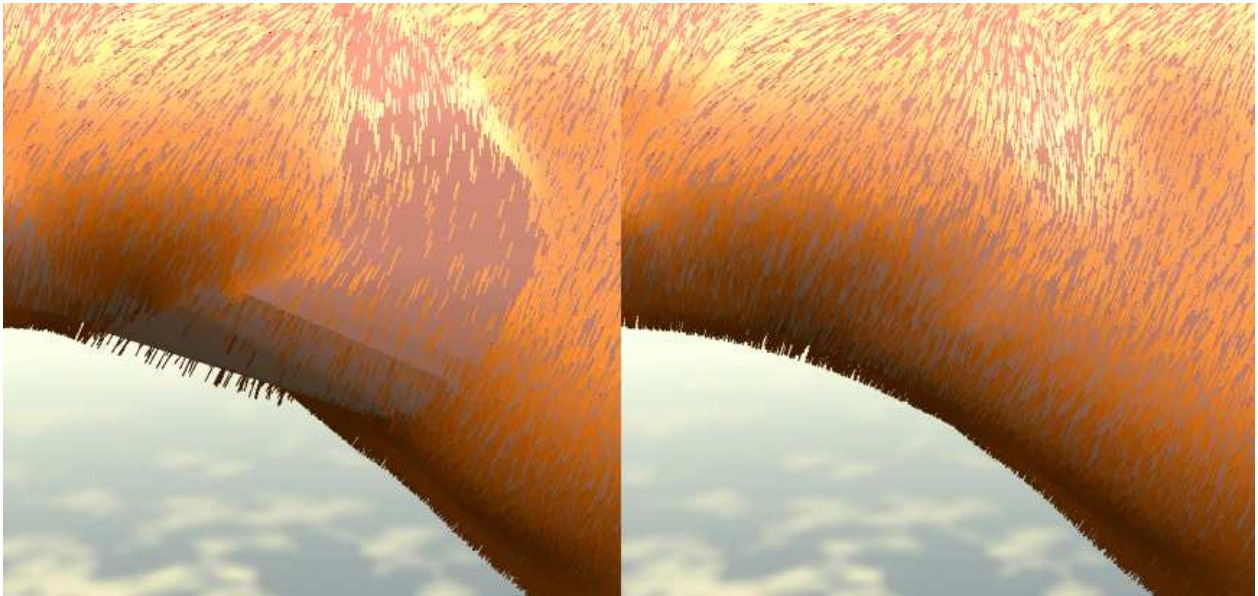


Figure 9: This figure illustrates the same effect as the previous two Figures 7 and 8 when fur is attached to skin triangles. In the left figure, the unequal stretching of the skin produces gaps in the fur, as well as irregularities in the skin surface. On the right, the fur and skin appear normal.

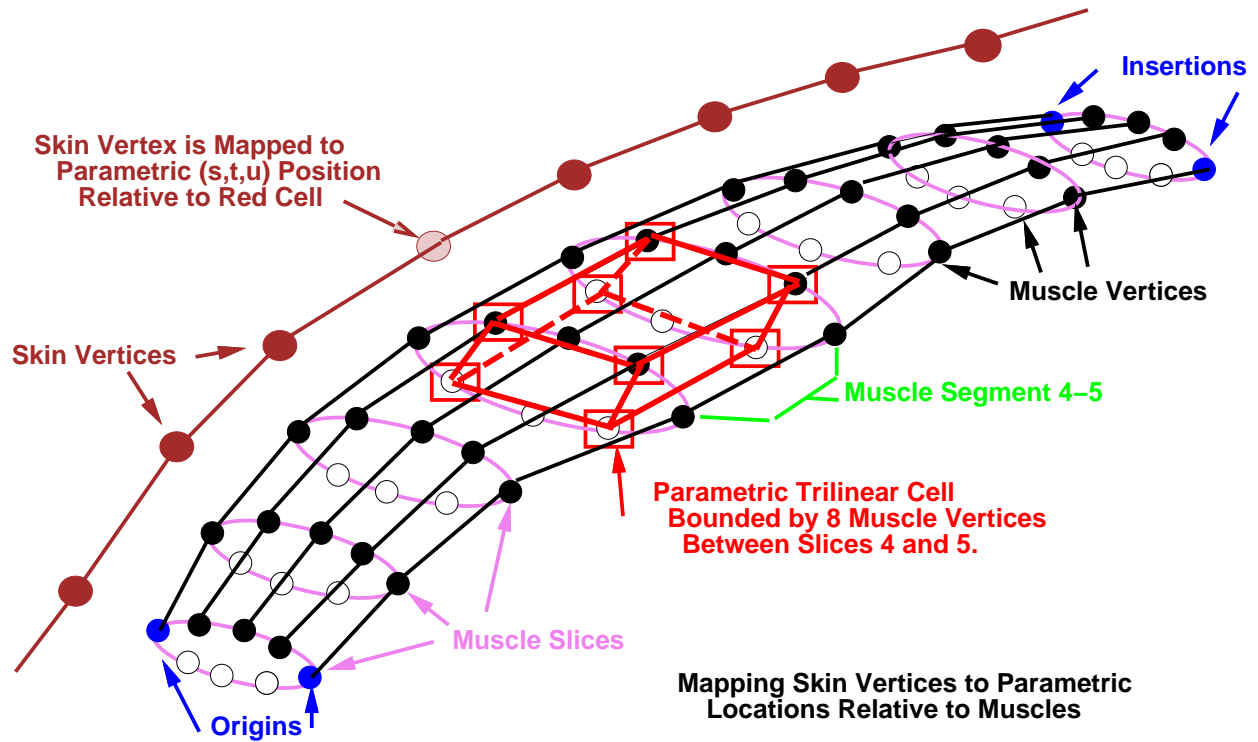


Figure 10: Illustration of mapping skin vertices to parametric trilinear functions over muscle segments. The lightest skin vertex lies between muscle slices 4 and 5, and is mapped into an (s, t, u) coordinate system defined by the eight muscle vertices shown in red.



Figure 11: These three monkeys were made from the identical underlying components and skin as all the other monkeys in the paper. but in the left image the arms are lengthened, in the right image the legs are lengthened, and in the center the skin thickness is increased.

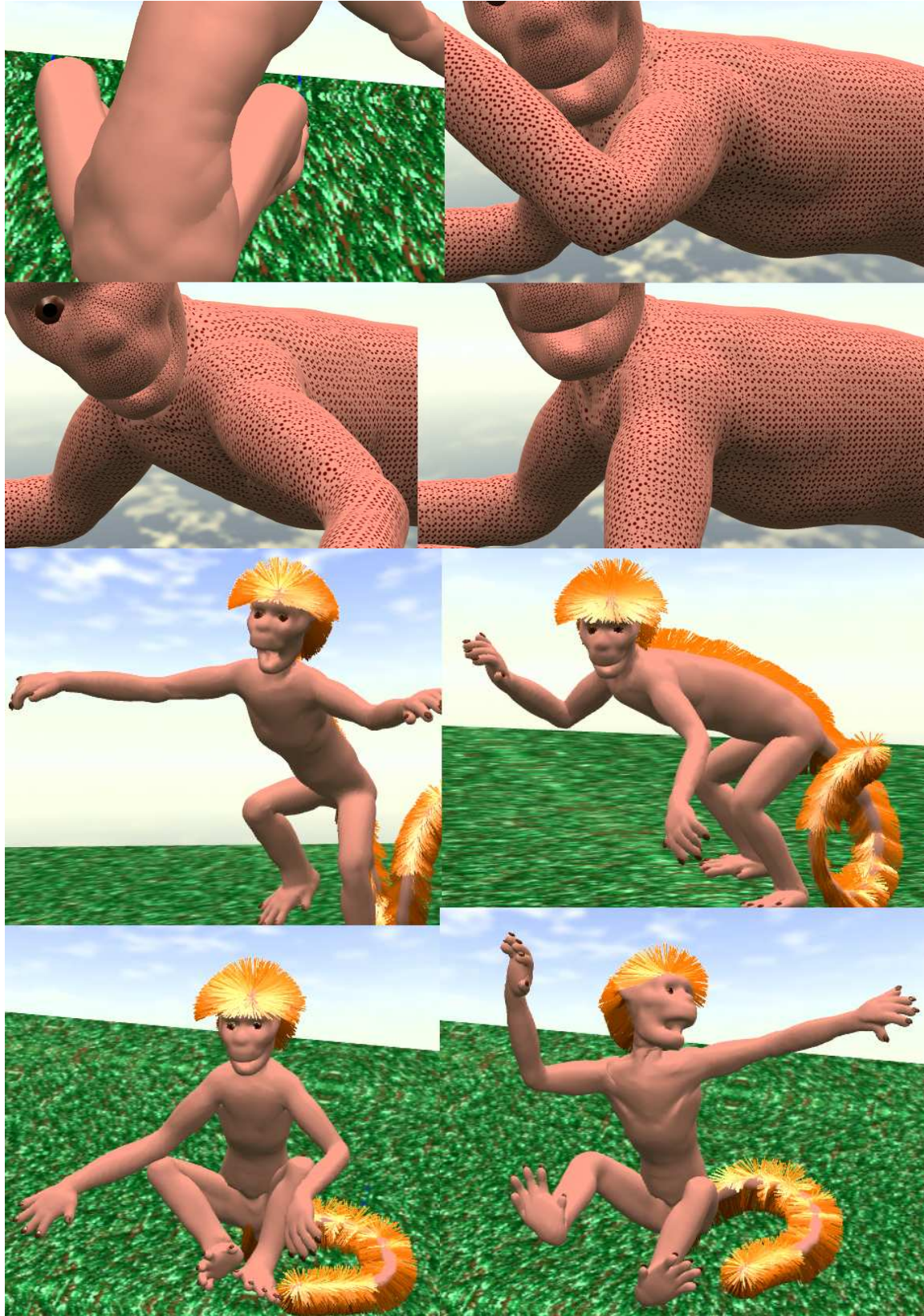


Figure 12: A selection of monkey images. Notice the effect of individual muscles, and the ability of the model to simulate both stretching and folds.